Self-perpetuating Carbon-foam Microwave Plasma Conversion of Hydrocarbon Wastes into Useful Fuels and Chemicals

Guiyin Xu¹, Haibin Jiang¹, Myles Stapelberg¹, Jiawei Zhou², Mengyang Liu³, Qingjie Li¹, Yunteng Cao⁴, Rui Gao¹, Minggang Cai³, Jinliang Qiao^{*5}, Mitchell S Galanek⁶, Weijiang Xue¹, Benedetto Marelli⁴, Meifang Zhu^{*7}, Ju Li^{*1,8}

⁵ SINOPEC Beijing Research Institute of Chemical Industry, Beijing 100013, China

Abstract

White wastes (unseparated plastics, facemasks, textiles, etc.) pose a serious challenge to sustainable human development and the ecosystem, and have recently been exacerbated due to the surge in plastics usage and medical wastes from COVID-19. Current recycling methods such as chemical recycling, mechanical recycling, and incineration require either pre-sorting and washing, or releasing CO₂. In this work, a carbon foam microwave plasma (CFMP) process is developed, utilizing plasma discharge to generate surface temperatures exceeding ~3000 Kelvin in an N₂ atmosphere, to convert *unsorted* white wastes into gases (H₂, CO, C₂H₄, C₃H₆, CH₄, etc.) and small amounts of inorganic minerals and solid carbon, which can be buried as "coal". The process is self-perpetuating, as the new solid carbon asperities grafted onto the foam's surface actually increases the plasma discharge efficiency over time. This process has been characterized by *in-situ* optical probes and infrared sensors and optimized to handle most forms of white waste without the need for pre-sorting or washing. Thermal measurement and modeling show that in a flowing reactor, the device can achieve locally extremely high temperatures, but the container wall will still be cold and can be made with cheap material, and thus miniaturization of the waste incinerator is possible that also takes advantage of intermittent renewable electricity.

¹ Department of Nuclear Science and Engineering, Massachusetts Institute of Technology, Cambridge, MA 02139, USA

² Department of Mechanical Engineering, Massachusetts Institute of Technology, Cambridge, MA 02139, USA
³ College of Ocean & Earth Sciences, Xiamen University, Xiamen 361102, China

⁴ Department of Civil and Environmental Engineering, Massachusetts Institute of Technology, Cambridge, MA 02139, USA

⁶ Environment, Health & Safety Office, Massachusetts Institute of Technology, Cambridge, MA 02139, USA

⁷ State Key Laboratory for Modification of Chemical Fibers and Polymer Materials, College of Materials Science and Engineering, Donghua University, Shanghai 201620, China

⁸ Department of Materials Science and Engineering, Massachusetts Institute of Technology, Cambridge, MA 02139, USA

White wastes are now everywhere and range from food packaging (Figure S1a) to used facemasks/textiles (Figure S1b) to electronic device components such as battery separators (Figure S1c). The production of white wastes is increasing, with little hope to reach a global "peak waste" production before 2100. Disposal of white wastes is becoming a pressing issue with several of the world's largest landfills already beginning to reach their limits. The COVID-19 pandemic has only exacerbated the problem, by increasing the reliance on plastic goods and personal protective equipment (PPE) to contain the spread of the virus. Poorly stored and littered white wastes can be easily transported into the ocean by wind and rain. For example, 8 million metric tons of plastic enter the ocean every year and pose a grave threat to marine life (Figure S1d). These long-lasting debris take up to 500 years to bio-degrade in the ocean. Microplastics formed by weathering and bio-degradation (Table S1, 2)6.7 are often detected in estuaries, lakes, coastal waters, beaches, and could also be found in the deep-sea sediments, ice cores and Arctic & Antarctic waters (Figure S2, S3). 6.8-11

The current recycling methods used are mechanical and chemical recycling, with both methods limited to processing only polyethylene and poly(ethylene terephthalate) PET at an industrial scale. 12,13 Chemical recycling also requires sorting processes to separate white wastes into pure feedstocks. 14 Furthermore, catalysts limit the efficiency and selectivity of chemical recycling. These processes call for large capital equipment and centralized processing plants, and transportation of distributed white wastes to these large plants incur additional costs. A local community level treatment of white wastes that do not require mechanical sorting and take advantage of intermittent renewable electricity would be highly desirable. 15,16

White wastes are mostly long-chain hydrocarbons, and in reducing atmosphere at high temperatures, will decompose into H₂, CO, C₂H₄, C₃H₆, CH₄, etc. These gases plus residual solid carbon C_n are valuable ingredients for the chemical industry, acting as feedstock to make fresh plastics and other useful chemicals. It is essential that solid carbon C_n components are not oxidized in the process, as that would produce unwanted CO₂ emission. This residual carbon should also be well contained, as it would become another source of pollution in the form of soot. Finally, inorganic components such as dyes or fillers, like SiO₂ and Al₂O₃, are unavoidable in real waste and must be collected as compact solid waste. With standard incineration, not only would one

generate CO₂ greenhouse gas, but these unavoidable inorganic residues would become airborne particulates that contribute to PM 2.5 in haze. The optimal recycling process should thus be:

Unsorted white wastes \rightarrow H₂, CO, C₂H₄, C₃H₆, CH₄, etc. gases + coal-like minerals (1)

converting waste into gaseous feedstock and stable coal-like solids. This would allow disposal of the C_n/SiO₂/Al₂O₃/... composites coal-like solids underground, such as an abandoned coal mine, ensuring the residual solids do not leach into the ground water. The gases collected (e.g. H₂) may be reformed to drive fuel cells or be sent to chemical factories (e.g. C₂H₄) *via* gas pipelines to make new plastics and chemicals, thus closing the materials loop, without stressing the road transportation network.

The standard approach to (1) requires large industrial installations and pressure vessels made with expensive alloys, due to the *uniformly* high temperatures (and thus pressure) involved. This present work proposes the use of microwave plasma discharge, where the local temperature can reach many thousands of Kelvin due to oscillating electromagnetic fields, while maintaining ambient temperatures within the reactor chamber. This alternative method could forego the expensive pressure vessels and instead rely upon cheaper materials such as those found in household microwave ovens. Microwave ovens create standing-wave electromagnetic radiation in the frequency range of 300 MHz to 300 GHz.¹⁷ Due to itinerant electrons in the carbon foam and incident microwaves, a large electric field can form on the surface of the foam, inducing gas plasma discharge, ionizing nearby N₂ gas and generating local temperatures in excess of 3000K.

Herein, a carbon foam microwave plasma (CFMP) process was developed to generate high local temperatures to transform white wastes into hydrogen gas and useful chemicals like ethylene (C₂H₄), propylene (C₃H₆), and methane (CH₄). While plasmas can promote various kinds of chemical reactions by creating free radicals, ions, and high temperatures in ambient conditions, the process to form plasma discharge is not straightforward. Current state of the art techniques utilize refractory metals like tungsten (W) to induce plasma discharge. Graphitic carbon, a cheaper alternative, is another possibility due to its high sublimation temperatures. In this work, it is shown that exposing an appropriately designed carbon foam to nitrogen gas and microwaves can induce plasma discharging, forming a nitrogen plasma. During this short and localized process,

plasmas decompose the white wastes into H-bearing small gas molecules, with excess high-quality graphitic carbon precipitating out as solid C_n grafted onto the pre-existing foam, forming a self-perpetuating "carbon foam cycle". A small amount of CO could also be generated due to trace amounts of oxygen in the atmosphere and oxygen from the original polymer. Surprisingly, C_n is deposited on the surface of the carbon foam, forming electrically conductive barbed tips that facilitate further discharge, so much so that efficiency of the foam increases over time. To address the growing consumption of plastic goods and COVID-19, we propose CFMP as a method to recycle white wastes without the need for pre-sorting and cleaning, lowering the costs attributed to recycling and reducing the number of steps from waste to fuels and chemicals.

Experimental Setup

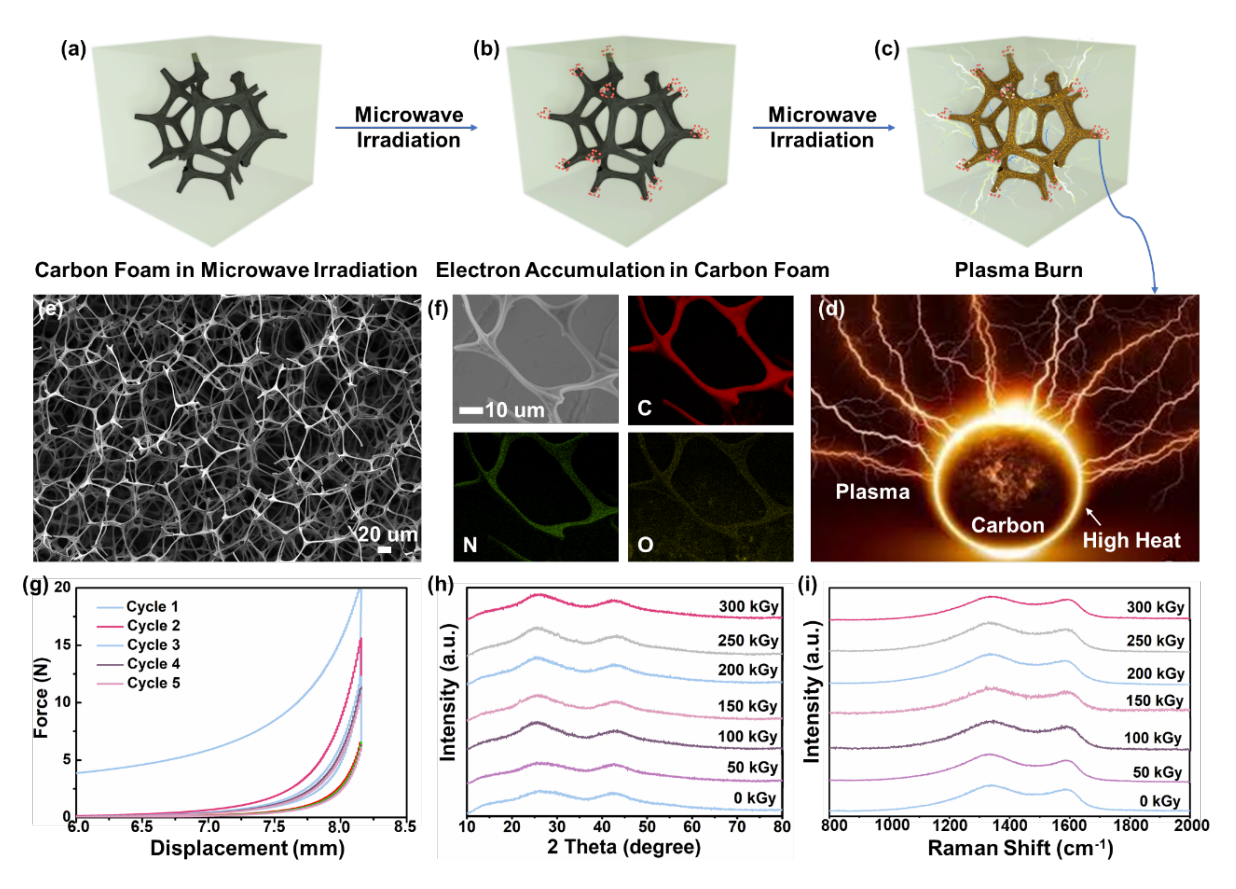


Figure 1. (a-d) Schematic illustration of the plasma burn and heat production by the carbon foam in the microwave irradiation. Figure 2d taken from https://www.theepochtimes.com/did-a-giant-cosmic-lightning-bolt-hit-mars-could-one-hit-earth_899276.html (e) Scanning electron microscopy (SEM) image of the carbon foam. (f) Scanning transmission electronic microscope (STEM) image of the carbon foam and the corresponding elemental mapping images for carbon, nitrogen, and oxygen. (g) Cyclic stress-strain curves of the carbon foam. (h) X-ray diffraction (XRD) patterns and (i) Raman

spectrum of the carbon foam irradiated at different kGy doses (0, 50, 100, 150, 200, 250, 300 does).

In this work, a carbon foam was used to induce plasma discharge with microwave irradiation (**Figure 1a-d**). The carbon foam was initially produced by the thermal decomposition of commercial melamine foams in nitrogen, with yield up to 60wt% (**Figure S4**). A distinct weight loss from ~400 °C is shown in the thermal gravimetric (TG) curve, corresponding to the escape of H and C atoms from the melamine. The TG weight curve stabilized after a heat temperature at 900 °C, indicating that a complete transformation of melamine to carbon had occurred. Carbon foam has a structure akin to a 3D barbed pentagonal honeycomb (**Figure 1e, Figure S5a, b**). Due to the removal of H and C atoms from the melamine, the surface of the carbon foam was porous (**Figure S5c**). High-resolution transmission electron microscopy (HRTEM) images show abundant micropores and mesopores within the foam (**Figure S5d**), measuring a Brunauer-Emmett-Teller (BET) surface area of 36.32 m² g⁻¹, pore volume of 0.06 cm³ g⁻¹, and average pore size of 6.15 nm (**Table S3**).

X-ray photoelectron spectroscopy (XPS) and scanning transmission electron microscopy (STEM) results verify a uniform distribution of carbon, nitrogen, and oxygen in the carbon foam (Figure 1f, Figure S6). The apparent bulk electrical conductivity of the carbon foam is ~3 S m⁻¹, which considering its high porosity (nominal density ~5 mg cm⁻³, thus porosity ~99.6%), suggests a very high electric conductivity at the microscopic level. Moreover, the carbon foam also demonstrates sufficient mechanical properties (Figure 1g, Video S1). Even under extreme conditions, such as exposure to gamma-ray irradiation (50-300 kGy), the carbon foam structure remained stable and its physical surface properties showed minimal changes (Figure S7-14, Table S3). X-ray diffraction (XRD) patterns are shown in **Figure 1h**, where the two broad signals around 26° and 44°, correspond to the (002) and (100) spacing of the graphene sheets, respectively. For the first peak at 26°, the intensity remained unchanged after 50 kGy of gamma irradiation. After 100 kGy, the intensity of the peak increased slightly, but then remained constant after exposure to 150, 200, 250, and 300 kGy. The peak at 44°, showed nominal changes in intensity after exposure to gamma irradiation. The Raman spectra in Figure 1i shows two strong bands at ~1590 and 1330 cm⁻¹, corresponding to the G-band and the disorder induced D-band. There are few changes of these peaks after the gamma irradiation is exposed on the carbon foam. This indicates that the carbon foam catalyst will be stable under microwave irradiation for extended periods of time.

The carbon foam utilizes plasma discharging to generate high local temperatures within the microwave oven. The process is as follows: after the carbon foam absorbs incident microwaves, electrons/holes accumulate at the asperities of the carbon foam (**Figure 1b**). With the accumulation of free electrons, high local electrical fields are then generated. Next, the accumulated electrons begin to emit into free space as cathodic ray emissions, and these electrons ionize the nitrogen gas, that set off a cascade of charged-particles ionizations, accelerations, and collisions under the electric field. Once plasma discharging occurs, the plasma is formed (**Figure 1c**), resulting in high temperatures on the surface of carbon foam (**Figure 1d**), and sending out bright lights (see Videos **S2-S3**).

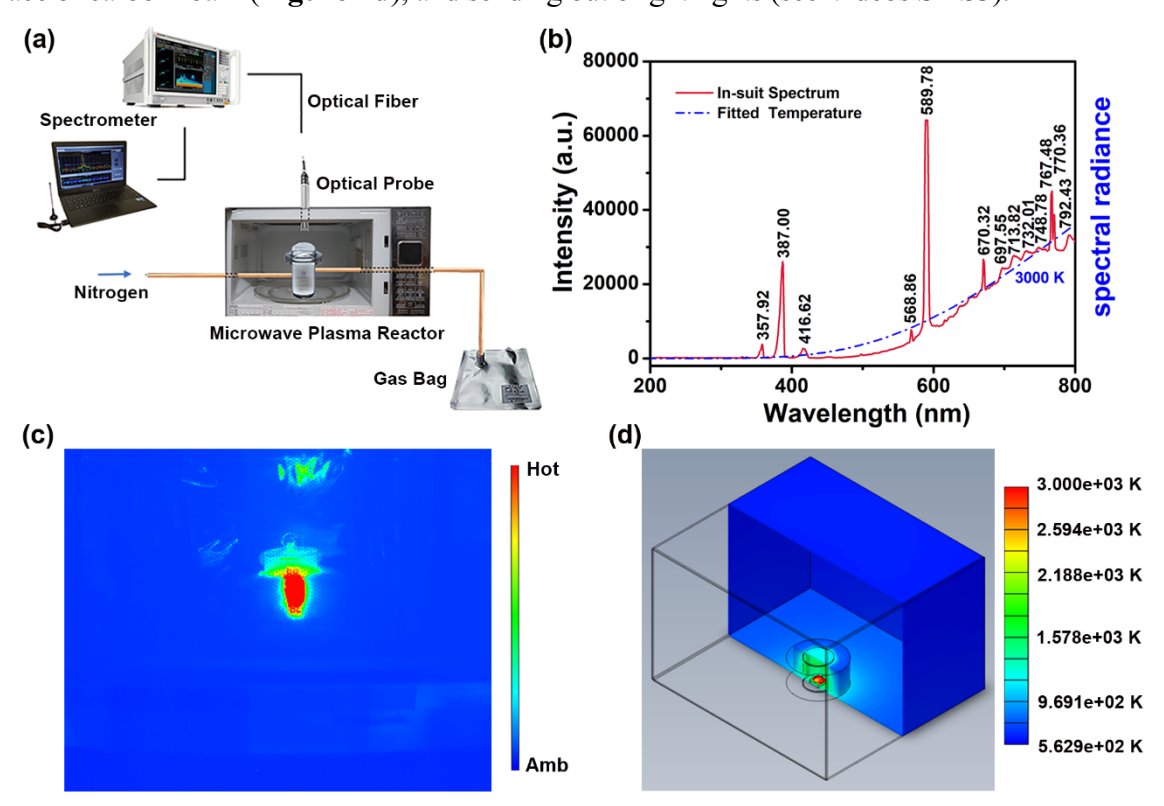


Figure 2. (a) Schematic illustration of the *in-suit* spectrum measurement system for the microwave plasma reactor. (b) The *in-suit* spectrum and fitted temperature of carbon foam in the microwave irradiation. (c) The *in-situ* temperature distribution of the microwave plasma reactor by a forward-looking infrared camera. The linear color scale represents the ambient and hot temperature. Absolute values of temperature are not reported due to the existence of microwave oven door in the viewing direction. (d) Steady-state thermal analysis simulated with SolidWorks.

Due to the high heating rates and temperatures involved in this nitrogen microwave plasma process, it is not easy to measure the reaction temperature. An *in-situ* spectral measurement system was used to indirectly estimate the temperature (**Figure 2a**). The peaks on this spectrum radiance plot correspond to the electronic transitions between the different energy levels in the carbon foam and nitrogen gas

(**Figure 2b**).²⁶ The peaks at 387.00 and 589.78 nm correspond to the transitions of $2s^22p4p$ to $2s2p^2(^4P)3p$ and $2s2p^2(^4P)3s$ to $2s2p^2(^4P)3p$ in nitrogen, respectively (**Table S4**). The peak located at 357.92 nm is attributed to the transition of $2s2p(^3P^\circ)3p$ to $2s2p(^3P^\circ)4s$ in carbon. The high lattice energy in the solid phase show that the peak intensity of nitrogen is higher than that of carbon. Overall, the spectrum radiance complies well with the Planck's law of black-body radiation²⁷:

$$B_{v}(T) = \frac{2hv^{3}}{c^{2}} \frac{1}{e^{\frac{hv}{kT}} - 1}$$
 (2)

where v is the frequency of the electromagnetic radiation; $B_v(T)$ is the spectral radiance density of frequency v radiation; T is the absolute temperature of the body; h is the Planck constant; c is the speed of light in a vacuum; k is the Boltzmann constant. By proper scaling and least-square regression on the measured spectrum radiance, we estimate that the microwave plasma process generates a temperature of 3000 K in a few seconds. The local high temperature enables the decomposition of even very stable organic wastes. The local high temperature was recorded by an in-situ infrared (IR) sensor (Figure S15, Figure 2c, Video S2). During the process, a high temperature region localized around the sample surface (at the center of the microwave plasma reactor) is observed after a few seconds. This suggests that the surface of the carbon foam, when exposed to the microwave plasma process, can serve as an effective medium for waste pyrolysis. Since high local temperatures are generated, ceramic fiber blankets were used to insulate the CFMP system (Figure S16a, b, Video S3). While a decrease in thermal emission from the microwave oven door limits our capability to quantify absolute temperature scales, it is clear that highly localized heat zones are generated on the carbon foam surface.

Thermal analysis on the microwave reactor designed in this work was done to understand temperature profiles during steady state operation, as an industrial system would likely be designed to run continuously to maximize productivity. The thermal analysis was calculated using SolidWorks Simulation, which employs the Stefan-Boltzmann equation for radiation heat transfer at steady state.

$$q = \epsilon \sigma A T^4 \tag{3}$$

where ε is the emissivity of an object, σ is the Stefan-Boltzmann constant, A is the area of the object radiating heat, and T is the temperature of the object. SolidWorks makes the distinction between surface to surface and surface to ambient radiative heat transfer by introducing a view

factor term, F, into **Equation 2**. This view factor is calculated based on meshing and user input and ranges from 0-1.

Figure 2d and Figure S17a show the side and top cutouts of the thermal analysis with a temperature bar showing the absolute temperatures within the system. This simulation is run at steady state and acts as an overestimate for the prototype environment tested in this work. The thermal insulation does an adequate job of containing the extreme temperatures generated by the carbon foam, while also maintaining an environment hot enough within the beaker to vaporize the plastics inserted. Figure S17b and Figure S17c show the side and top down profiles as well, but do so by cutting the system in half at the Z and Y axes, respectively. The side profile shows the temperature distribution for the system when run continuously, giving insight into what the maximum temperatures would be during operation. In the top view cutout, the bottom panel of the microwave would experience temperatures exceeding 800 K, due to the lack of convective heat transfer enacting on that panel, as the microwave is assumed to be placed on a table. This could be rectified by placing a ceramic fiber blanket under the quartz container, or by increasing gas flow to the bottom panel and raising the microwave several inches off its table. Implementing these small fixes could enable the safe, continuous operation of the CFMP, without relying on expensive high-temperature vessels and complicated thermal management systems.

Results and Discussions

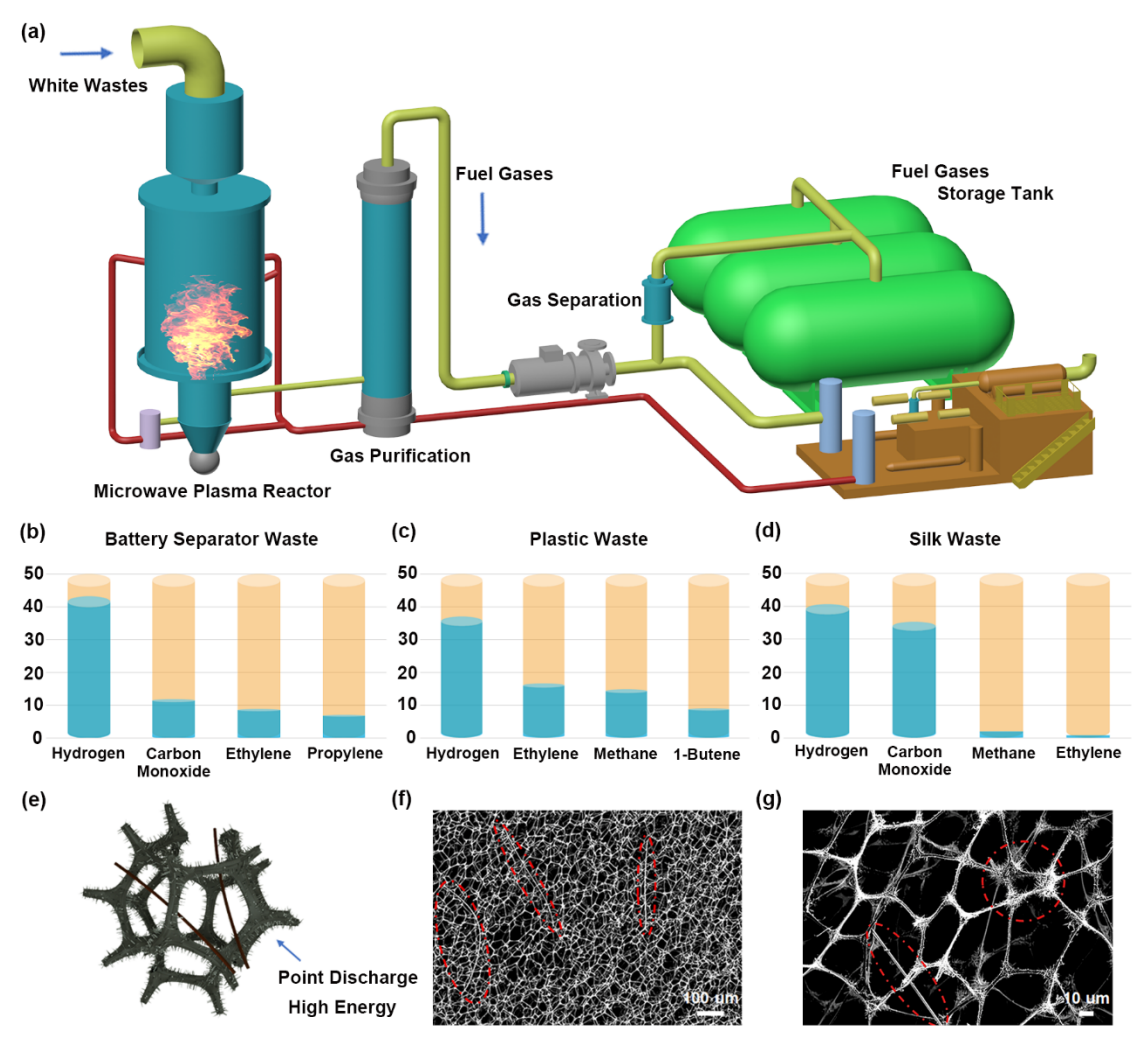


Figure 3. (a) The diagram of the industrial process for the white waste treatment by the carbon foam microwave plasma. The main gas composition (vol%) of (b) plastic waste, (c) batteries separator waste, and (d) silk waste by the carbon foam and microwave irradiation. The more detailed gas composition is shown in **Table S5**. (e) The schematic diagram of the carbon foam after the microwave irradiation for the batteries separator waste treatment. (f, g) Scanning electron microscopy (SEM) images of the carbon foam with batteries separator waste after the microwave irradiation of 330 W and 8 s.

The number of steps taken from white wastes to recycled industrial materials are drastically pared down with the CFMP process. White wastes are first cut into pieces to expose more surface area to the plasma and enhance the overall energy utilization of the system (**Figure 3a**). The brokendown wastes are then transferred into the microwave plasma reactor to be vaporized into reagents (H₂, CO, *etc.*) and separated into different storage tanks according to their chemical composition. Hydrogen-carbon monoxide products can then be directly fed into the Fischer-Tropsch process to synthesize chemical products.²⁸

In addition to plastics and silks, the fast development of lithium ion batteries for electric vehicles and

grid-scale energy storage, ^{29,30} has necessitated the accommodation of battery separators in the CFMP process. To recycle this more complicated class of waste, the CFMP reactor was used to pyrolyze the multicomponent separator polymers without pre-sorting. The output power of the microwave and the reaction time were discussed in supporting information **Figure S18-22**. For all experiments, a subsecond intermittence period of no microwaves was present, due to the design of our consumer microwave oven. A reaction time of 8 s was selected with varying output powers (110 W, 220 W, 330 W) for our initial experiments. At 110 W (**Video S4**), the battery separator waste only shrank on the surface of the carbon foam (**Figure S18a-c**). At 220 W (**Video S5**), residual amounts of battery separator waste remained (**Figure S19a-c**). However, at 330 W (**Video S6**), the surface of the carbon foam was clean (**Figure S20a-c**). After establishing the optimal output power (330 W), multiple reaction times (4, 8, 12 s) were tested. After 4 s (**Video S7, Figure S21a-c**), the result was similar to the 220 W, 8 s trial, and showed an insufficient treatment of the battery waste. At 12 s (**Video S8, Figure S22a-c**), an experimental result similar to 330 W, 8 s was observed.

In addition to battery separators, plastics, and silks, different types of facemasks were successfully treated by CFMP (**Figure S23**), demonstrating a promising recycling method to handle the surge in medical wastes due to COVID-19.

Gases obtained from white wastes using CFMP were analyzed with gas chromatography-mass spectrometry (GC-MS). Battery separator wastes yielded the following: 43.31 vol% hydrogen gas; 11.88 vol% carbon monoxide; 8.86 vol% ethylene; 7.10 vol% propylene, and 4.50 vol% methane (**Figure 3b, Table S5**). Plastic wastes yielded: 37.07 vol% hydrogen gas; 16.58 vol% ethylene; 14.89 vol% methane; 8.99 vol% 1-butene; 5.85 vol% propylene; and 4.61 vol% carbon monoxide respectively (**Figure 3c, Table S5**). Silk wastes yielded: 40.68 vol% hydrogen gas, 35.43 vol% carbon monoxide, 2.14 vol% methane, 0.83 vol% ethylene, respectively (**Figure 3d, Table S5**). The GC-MS results demonstrate that CFMP is an effective way to convert white wastes into useful fuel gases.

After each trial, residual carbon from the CFMP reaction was deposited on the carbon foam (**Figure 3e-g**). These are in the form of miniscule carbon fibers on the carbon foam (**Figure 3f**). While the barbed surface of the carbon foam remains intact after the CFMP process, carbon fuzzlike structures graft themselves on the surface of the carbon foam (**Figure 3g**). These fuzz sites improve the foam's ability to induce plasma discharge on the nitrogen gas by acting as an

additional site for electrons to accumulate at leap from (**Figure 3e, S22e**). While most catalysts deteriorate over time,²⁴ our CFMP catalyst improves, reducing the reliance on expensive metals and increasing the economic incentive to adopt this system for recycling white waste.

Conclusions

A miniaturizable, versatile method for recycling white wastes has been proposed and developed using a carbon foam-based microwave plasma reactor, that can be driven by intermittent renewable electricity. The CFMP process was studied and monitored in detail with GC-MS, an *in-situ* optical probe, and IR sensors. Initial experiments demonstrate the capability of CFMP to process white wastes into useful industrial regents, with hydrogen gas yields of up to 43.31 vol%. Additionally, the CFMP process can be used as a feeder for the Fischer-Tropsch process to convert white wastes into hydrocarbons such as ethanol, diesel, and natural gasses. The formation of graphitic carbon and plasma discharge constitutes a self-perpetuating chain reaction. CFMP's reliance upon cheap materials and its ability to process multiple plastics at once addresses major issues inherent in both chemical and mechanical recycling. This method should be applicable to other organic and mixed organic-inorganic wastes as well.

Methods

Preparation of carbon foam

Carbon foams were obtained from melamine foam by a high-temperature calcination at 900 °C for 2 h with a heating rate of 3 °C min⁻¹ in nitrogen.

Treatment of white wastes

Battery separator wastes were obtained from cycled coin cells in our lab. The Celgard lithium-ion battery separator films consisted of 25 µm trilayer polypropylene-polyethylene-polypropylene membranes. Plastic and silk wastes were from the abandoned bottles (polypropylene) and fabrics (silk fabric). These white wastes were treated on the carbon foam with a microwave plasma reactor at different length scales and power outputs. The microwave oven operated at a microwave frequency of 2.45 GHz and a maximum output of 1100 W (Panasonic, NN-SU696S).

Materials Characterization

Scanning electron microscopy (SEM) and scanning transmission electron microscopy (STEM) was performed on a Zeiss Merlin high-resolution SEM. Thermogravimetric analysis (TGA) was performed on a NETZSCH STA 409 PC TGA-DSC instrument under an N2 atmosphere at a heating rate of 10 °C min⁻¹ from 30-900 °C. Transmission electron microscopy (TEM) was carried out on a JOEL 2010F model. Compression experiments were carried out on a dynamic mechanical analysis (DMA) Q850 model (TA instruments, New Castle, DE) with a loading speed of 0.5 mm min⁻¹ at room temperature, and 3 samples were tested in total for repeatability. X-ray photoelectron spectroscopy (XPS) analysis was performed on a Perkin-Elmer PHI 550 spectrometer with AlKα radiation (1486.6 eV) as the X-ray source. Gamma irradiation measurements were conducted on a Gammacell Irradiator (220 Excel self-shielded high dose rate gamma ray). The N₂adsorption/desorption tests were determined by using Brunauer-Emmett-Teller (BET) measurements on an ASAP-2010 surface-area analyzer. Pore-size distribution (PSD) was derived from the adsorption branch of the isotherm by using the Barrett-Joyner-Halenda (BJH) method. The X-ray diffraction (XRD) patterns were recorded on a Bruker-AXS D8 DISCOVER. Room temperature Raman spectroscopy was conducted with a Jobin Yvon HR800 confocal Raman system with a 632.8 nm diode-laser excitation on a 300 S mm⁻¹ line grating. *In-situ* light spectrum data was recorded on a FX2000-EX type fiber optic spectrometer. Gas products were analyzed with a refinery gas analyzer (HP Agilent 7890 A).

Simulation

All parts made in SolidWorks were treated as solid bodies and included the following materials from the software's database: Glass (for the beaker), Copolymer (for the plastic/mask sample), and Plain Carbon Steel (for the microwave enclosure). Two custom materials were implemented: ceramic insulation based on FiberFax® and Carbon Foam. Further improvement of the thermal analysis, from a materials selection perspective, could be made with more exact thermal properties for the carbon foam. However, besides convection from the outside of the microwave to the ambient region, radiation is assumed to be the main mechanism for heat transfer. Therefore, according to *Equation* 3, temperature and exposed areas are the driving factors for this analysis. Further information such as the part shapes, material properties, mesh information, and thermal loads are summarized in **Table S6-12**.

References

- Hoornweg, D., Bhada-Tata, P. & Kennedy, C. Environment: Waste production must peak this century. *Nature* **502**, 615–617, doi:10.1038/502615a (2013).
- 2 You, S., Sonne, C. & Ok, Y. S. COVID-19's unsustainable waste management. *Science* **368**, 1438-1438, doi:10.1126/science.abc7778 (2020).
- 3 <u>https://www.weforum.org/agenda/2020/07/plastic-waste-management-covid19-ppe/.</u>
- Jambeck, J. R. *et al.* Plastic waste inputs from land into the ocean. *Science* **347**, 768-771, doi:10.1126/science.1260352 (2015).
- 5 <u>https://www.statista.com/chart/15905/the-estimated-number-of-years-for-selected-items-to-bio-degrade/.</u>
- de Souza Machado, A. A., Kloas, W., Zarfl, C., Hempel, S. & Rillig, M. C. Microplastics as an emerging threat to terrestrial ecosystems. *Global Change Biology* **24**, 1405-1416, doi:10.1111/gcb.14020 (2018).
- Auta, H. S., Emenike, C. U. & Fauziah, S. H. Distribution and importance of microplastics in the marine environment: A review of the sources, fate, effects, and potential solutions. *Environment international* **102**, 165-176, doi:10.1016/j.envint.2017.02.013 (2017).
- 8 Lusher, A. L., Tirelli, V., O'Connor, I. & Officer, R. Microplastics in Arctic polar waters: the first reported values of particles in surface and sub-surface samples. *Scientific Reports* 5, 14947, doi:10.1038/srep14947 (2015).
- 9 Eriksen, M. *et al.* Microplastic pollution in the surface waters of the Laurentian Great Lakes. *Mar Pollut Bull* **77**, 177-182, doi:10.1016/j.marpolbul.2013.10.007 (2013).
- Isobe, A., Uchiyama-Matsumoto, K., Uchida, K. & Tokai, T. Microplastics in the Southern Ocean. *Mar Pollut Bull* **114**, 623-626, doi: https://doi.org/10.1016/j.marpolbul.2016.09.037 (2017).
- Mu, J. *et al.* Microplastics abundance and characteristics in surface waters from the Northwest Pacific, the Bering Sea, and the Chukchi Sea. *Mar Pollut Bull* **143**, 58-65, doi:https://doi.org/10.1016/j.marpolbul.2019.04.023 (2019).
- Garcia, J. M. & Robertson, M. L. The future of plastics recycling. *Science* **358**, 870-872, doi:10.1126/science.aaq0324 (2017).
- Rahimi, A. & García, J. M. Chemical recycling of waste plastics for new materials production. *Nature Reviews Chemistry* **1**, 0046, doi:10.1038/s41570-017-0046 (2017).
- Ressourceneffizienz, V. Z. Recycling plastics Resource efficiency with an optimized sorting method. https://www.youtube.com/watch?v=I_fUpP-hq3A (2018).
- 15 Guha Roy, A. Detailing plastic pollution. *Nature Sustainability* **2**, 654-654, doi:10.1038/s41893-019-0367-2 (2019).
- Zhang, Z. *et al.* Recovering waste plastics using shape-selective nano-scale reactors as catalysts. *Nature Sustainability* **2**, 39-42, doi:10.1038/s41893-018-0195-9 (2019).
- 17 <u>https://en.wikipedia.org/wiki/Microwave_oven#cite_note-1</u>.
- Hawtof, R. *et al.* Catalyst-free, highly selective synthesis of ammonia from nitrogen and water by a plasma electrolytic system. *Science Advances* **5**, eaat5778, doi:10.1126/sciadv.aat5778 (2019).
- Sun, J. *et al.* Novel treatment of a biomass tar model compound via microwave-metal discharges. *Fuel* **207**, 121-125, doi: https://doi.org/10.1016/j.fuel.2017.06.075 (2017).
- 20 Khattak, H. K., Bianucci, P. & Slepkov, A. D. Linking plasma formation in grapes to

- microwave resonances of aqueous dimers. *Proceedings of the National Academy of Sciences* **116**, 4000-4005, doi:10.1073/pnas.1818350116 (2019).
- Xu, S. *et al.* Uniform, Scalable, High-Temperature Microwave Shock for Nanoparticle Synthesis through Defect Engineering. *Matter* **1**, 759-769, doi:https://doi.org/10.1016/j.matt.2019.05.022 (2019).
- Wang, W. *et al.* Experimental Study of Microwave-Induced Discharge and Mechanism Analysis Based on Spectrum Acquisition. *IEEE Transactions on Plasma Science* **45**, 2235-2242, doi:10.1109/TPS.2017.2715800 (2017).
- Huang, H. *et al.* Rapid and energy-efficient microwave pyrolysis for high-yield production of highly-active bifunctional electrocatalysts for water splitting. *Energy & Environmental Science* **13**, 545-553, doi:10.1039/C9EE03273H (2020).
- Sun, J. *et al.* Review on microwave–metal discharges and their applications in energy and industrial processes. *Applied Energy* **175**, 141-157, doi:https://doi.org/10.1016/j.apenergy.2016.04.091 (2016).
- Xu, G. *et al.* Biomass-derived porous carbon materials with sulfur and nitrogen dual-doping for energy storage. *Green Chemistry* **17**, 1668-1674, doi:10.1039/C4GC02185A (2015).
- 26 https://physics.nist.gov/PhysRefData/ASD/lines form.html.
- 27 <u>https://en.wikipedia.org/wiki/Black-body_radiation</u>.
- Lancet, M. S. & Anders, E. Carbon Isotope Fractionation in the Fischer-Tropsch Synthesis and in Meteorites. *Science* **170**, 980-982, doi:10.1126/science.170.3961.980 (1970).
- 29 Xu, G. *et al.* Ad hoc solid electrolyte on acidized carbon nanotube paper improves cycle life of lithium–sulfur batteries. *Energy & Environmental Science* **10**, 2544-2551, doi:10.1039/C7EE01898C (2017).
- Xu, G. *et al.* Exploring metal organic frameworks for energy storage in batteries and supercapacitors. *Materials Today* **20**, 191-209, doi:https://doi.org/10.1016/j.mattod.2016.10.003 (2017).

Acknowledgements

J.L. acknowledges the support by NSF ECCS-1610806.

Contributions

G.X., J.Q., and J.L. conceived the idea and experiments. G.X. prepared the carbon foam. G.X. and H.J. conducted the microwave plasma process. M.L. and M.C. analyzed the distribution of microplastics. J.Z, Y.C., R.G., Q.L., and W.X. carried out the material characterization. M.G. conducted the Gamma-cell Irradiator. G.X. analyzed the data and wrote the manuscript with M.S., M.Z., and J.L. All the authors participated in the manuscript reviewing.

Competing interests

The authors declare no competing interests.

Supplementary Information

Supplementary Figure S1-23, Video S1-8, and Table S1-12.